Design and laboratory tests of a Doppler Asymmetric Spatial Heterodyne (DASH) interferometer for upper atmospheric wind and temperature observations

John M. Harlander,[1,*] Christoph R. Englert,[2] David D. Babcock[3], and Frederick L. Roesler[4]

[1]*Department of Physics, Astronomy and Engineering Science, St Cloud State University, 720 Fourth Avenue South, St Cloud, Minnesota 56301, USA*
[2]*U.S. Naval Research Laboratory, Space Science Division, Code 7641, 4555 Overlook Avenue Southwest, Washington, District of Columbia 20375, USA*
[3]*Artep Inc., 2922 Excelsior Springs Court, Ellicott City, Maryland 21042, USA*
[4]*Department of Physics, University of Wisconsin–Madison, 1150 University Avenue, Madison, Wisconsin 57306. USA*
**jmharlander@stcloudstate.edu*

Abstract: We describe the design, fabrication and laboratory tests of a Doppler Asymmetric Spatial Heterodyne (DASH) interferometer for upper atmospheric wind and temperature observations of the O[^{1}D] 630 nm emission. The monolithic interferometer has no moving parts, a large étendue, relaxed fabrication and alignment tolerances and can measure multiple emission lines simultaneously. Laboratory measurements indicate that the design resolution and étendue were achieved and that thermal drifts can be determined with sufficient precision for geophysical applications.

©2010 Optical Society of America

OCIS codes: (010.0280) Remote sensing and sensors; (120.0280) Remote sensing and sensors; (280.4991) Passive remote sensing; (300.2140) Emission; (300.6190) Spectrometers; (300.6320) Spectroscopy, high-resolution.

References and links

1. T. L. Killeen, Q. Wu, S. C. Solomon, D. A. Ortland, W. R. Skinner, R. J. Niciejewski, and D. A. Gell, "TIMED Doppler Interferometer: Overview and recent results," J. Geophys. Res. **111**(A10), A10S01 (2006), doi:10.1029/2005JA011484.
2. P. B. Hays, V. J. Abreu, M. E. Dobbs, D. A. Gell, H. J. Grassl, and W. R. Skinner, "The High-Resolution Doppler Imager on the Upper Atmosphere Research Sateelite," J. Geophys. Res. **98**(D6), 10713–10723 (1993), doi:10.1029/93JD00409.
3. J. W. Meriwether, "Studies of thermospheric dynamics with a Fabry–Perot interferometer network: A review," J. Atmos. Sol. Terr. Phys. **68**(13), 1576–1589 (2006).
4. G. G. Shepherd, G. Thuillier, W. A. Gault, B. H. Solheim, C. Hersom, J. M. Alunni, J.-F. Brun, S. Brune, P. Charlot, L. L. Cogger, D.-L. Desaulniers, W. F. J. Evans, R. L. Gattinger, F. Girod, D. Harvie, R. H. Hum, D. J. W. Kendall, E. J. Llewellyn, R. P. Lowe, J. Ohrt, F. Pasternak, O. Peillet, I. Powell, Y. Rochon, W. E. Ward, R. H. Wiens, and J. Wimperis, "WINDII, the wind imaging interferometer on the upper atmosphere research satellite," J. Geophys. Res. **98**(D6), 10725–10750 (1993).
5. C. R. Englert, J. M. Harlander, J. T. Emmert, D. D. Babcock, and F. L. Roesler, "Initial ground-based thermospheric wind measurements using Doppler asymmetric spatial heterodyne spectroscopy (DASH)," Opt. Express. submitted.
6. J. M. Harlander, R. J. Reynolds, and F. L. Roesler, "Spatial heterodyne spectroscopy for the exploration of diffuse interstellar emission lines at far-ultraviolet wavelengths," Astrophys. J. **396**, 730–740 (1992).
7. C. R. Englert, J. M. Harlander, J. G. Cardon, and F. L. Roesler, "Correction of phase distortion in spatial heterodyne spectroscopy," Appl. Opt. **43**(36), 6680–6687 (2004).
8. C. R. Englert, M. H. Stevens, D. E. Siskind, J. M. Harlander, and F. L. Roesler, "The Spatial Heterodyne Imager for Mesospheric Radicals (SHIMMER) on STPSat-1," J. Geophys. Res. in press., doi:10.1029/2010JD014398.
9. J. M. Harlander, F. L. Roesler, J. G. Cardon, C. R. Englert, and R. R. Conway, "SHIMMER: a spatial heterodyne spectrometer for remote sensing of earth's middle atmosphere," Appl. Opt. **41**(7), 1343–1352 (2002).
10. C. R. Englert, D. D. Babcock, and J. M. Harlander, "Doppler asymmetric spatial heterodyne spectroscopy (DASH): concept and experimental demonstration," Appl. Opt. **46**(29), 7297–7307 (2007).

#137013 - $15.00 USD Received 22 Oct 2010; accepted 16 Nov 2010; published 1 Dec 2010
(C) 2010 OSA

Report Documentation Page

Form Approved
OMB No. 0704-0188

Public reporting burden for the collection of information is estimated to average 1 hour per response, including the time for reviewing instructions, searching existing data sources, gathering and maintaining the data needed, and completing and reviewing the collection of information. Send comments regarding this burden estimate or any other aspect of this collection of information, including suggestions for reducing this burden, to Washington Headquarters Services, Directorate for Information Operations and Reports, 1215 Jefferson Davis Highway, Suite 1204, Arlington VA 22202-4302. Respondents should be aware that notwithstanding any other provision of law, no person shall be subject to a penalty for failing to comply with a collection of information if it does not display a currently valid OMB control number.

1. REPORT DATE	2. REPORT TYPE	3. DATES COVERED
OCT 2010		**00-00-2010 to 00-00-2010**

4. TITLE AND SUBTITLE	5a. CONTRACT NUMBER
Design and laboratory tests of a Doppler Asymmetric Spatial Heterodyne (DASH) interferometer for upper atmospheric wind and temperature observations	5b. GRANT NUMBER
	5c. PROGRAM ELEMENT NUMBER
6. AUTHOR(S)	5d. PROJECT NUMBER
	5e. TASK NUMBER
	5f. WORK UNIT NUMBER
7. PERFORMING ORGANIZATION NAME(S) AND ADDRESS(ES) **Naval Research Laboratory,Space Science Division, Code 7641,4555 Overlook Ave SW,Washington,DC,20375**	8. PERFORMING ORGANIZATION REPORT NUMBER
9. SPONSORING/MONITORING AGENCY NAME(S) AND ADDRESS(ES)	10. SPONSOR/MONITOR'S ACRONYM(S)
	11. SPONSOR/MONITOR'S REPORT NUMBER(S)

12. DISTRIBUTION/AVAILABILITY STATEMENT
Approved for public release; distribution unlimited

13. SUPPLEMENTARY NOTES

14. ABSTRACT

We describe the design, fabrication and laboratory tests of a Doppler Asymmetric Spatial Heterodyne (DASH) interferometer for upper atmospheric wind and temperature observations of the O[1D] 630 nm emission. The monolithic interferometer has no moving parts, a large ?ndue, relaxed fabrication and alignment tolerances and can measure multiple emission lines simultaneously. Laboratory measurements indicate that the design resolution and ?ndue were achieved and that thermal drifts can be determined with sufficient precision for geophysical applications.

15. SUBJECT TERMS

16. SECURITY CLASSIFICATION OF:			17. LIMITATION OF ABSTRACT	18. NUMBER OF PAGES	19a. NAME OF RESPONSIBLE PERSON
a. REPORT **unclassified**	b. ABSTRACT **unclassified**	c. THIS PAGE **unclassified**	**Same as Report (SAR)**	**11**	

1. Introduction

Interference spectrometers have well-known advantages for obtaining spectra of faint, diffuse sources such as upper atmospheric airglow emissions. These measurements typically require high spectral resolution and sensitivity over a narrow spectral band. To date the instruments of choice have been Fabry-Perot [1–3] and wide-angle Michelson interferometers [4]. The technical difficulties associated with operating these interferometers, particularly in harsh environments such as on board orbiting spacecraft are challenging. Fabry-Perot interferometers have stringent optical flatness and alignment requirements while wide-angle Michelson interferometers, due to the limited number of optical path differences sampled, typically measure only single isolated emission lines. In response to these challenges, we have been developing a Doppler Asymmetric Spatial Heterodyne (DASH) technique that is optimized for measuring upper atmospheric winds and temperatures. A DASH is similar to a wide-angle Michelson; however, it measures many more path difference samples within a much larger path difference interval without moving parts. This feature enables the instrument to measure multiple atmospheric lines and to simultaneously monitor an on-board calibration line to track instrumental drifts. It is a two-beam interferometer with greatly relaxed optical flatness and alignment requirements when compared to both the Fabry-Perot and Michelson. The DASH interferometer described in this paper was designed for temperature and wind measurements of the upper atmospheric red line at 630 nm. For years this emission has been measured from the ground and space-based instruments to determine F-region winds and temperatures [1,2,4]. This particular red line DASH interferometer utilizes a Köster's prism as a beamsplitter to enable a quasi-common path configuration such that both arms use different parts of the same field-widening prism and diffraction grating. By choice of an appropriate prism glass, the interferometer was designed to be thermally compensated. In this paper we will discuss the design and laboratory tests of the interferometer. A companion paper [5] discusses the optics other than the interferometer, details of the data analysis and the first ground-based geophysical wind measurements of an instrument that includes this interferometer.

2. DASH Heritage: Spatial Heterodyne Spectrometer (SHS)

The DASH interferometer is a variant of the Spatial Heterodyne Spectrometer (SHS) concept. A detailed description of the SHS technique is given by Harlander et al. [6]. An SHS consists of a Michelson interferometer with the return mirrors replaced by fixed, tilted diffraction gratings. The addition of fixed field widening prisms [6] increases the possible throughput (étendue) by approximately two orders of magnitude over a conventional interferometer, making the system extremely sensitive for faint-diffuse source spectroscopy. The SHS optics produce a wavelength-dependent Fizeau fringe pattern localized near the gratings which is imaged on an array detector. Each wavelength in the incident spectrum produces a unique spatial fringe frequency, and the fringe pattern from a spectrally complex source is the Fourier Transform of the spectrum. Rather than sequentially scanning the path difference by moving a mirror as is done in a conventional Michelson the path difference is simultaneously sampled in the spatial domain by the array detector. Furthermore, the interferogram is "heterodyned" because the spatial fringe frequency for an incident wavenumber is proportional to the difference between this wavenumber and the Littrow wavenumber of the diffraction gratings. This feature enables the system to measure high resolution spectra about a limited spectral band with a limited number of interferogram samples, i.e. a limited number of detector elements. The system achieves the theoretical resolving power of the diffraction gratings (sum of the grooves on both gratings) but has a throughput characteristic of an interferometer [6]. The fringes are localized inside the interferometer so in addition to having no moving parts, the system is particularly immune to optical defects and misalignments because the interferometer elements are either imaged or nearly imaged on the detector. As a result, optical defects or misalignments will distort or shift the fringes but as long as the optical quality of the surfaces is good over the small area sampled by each detector pixel, the

#137013 - $15.00 USD Received 22 Oct 2010; accepted 16 Nov 2010; published 1 Dec 2010
(C) 2010 OSA

fringes are recorded with high contrast. With proper calibration the distorted fringes can be corrected in software [7]. SHS alignment tolerances are relaxed by at least a factor of 10 over Fabry-Perot and Michelson spectrometers where the interferometric optics are usually at the pupil of the system so that each detector element measures signal over the full interferometer aperture. To obtain high contrast fringes with these conventional interferometers the alignment and flatness must be maintained to sub-wavelength tolerances.

3. DASH concept

The above section indicates some of the features of SHS that make it particularly suited to space flight applications where mass, volume and sensitivity to misalignment are limiting design considerations [8–10]. One such application are limb observations of Doppler winds and temperatures from a low-altitude spacecraft. The spectra in these applications are often relatively simple, i.e. consisting of one or a few isolated, thermally broadened emission lines, especially for thermospheric altitudes.

Figure 1 illustrates the situation for a single thermally-broadened emission line. The fringes shown in the middle of the figure in light and dark gray are two interferograms with slightly different fringe frequencies corresponding to different wind speeds. Near zero path difference these interferograms are nearly identical; however, as the optical path difference (OPD) increases to the right of the figure the phase difference between them increases owing to their slightly different spatial frequency. The decrease in the fringe envelope with optical path difference is due to the linewidth of the source. Higher temperatures result in increased broadening of the line and a more rapid decrease in fringe modulation with increasing path difference.

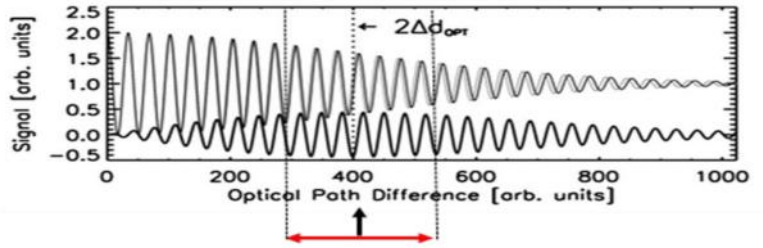

Fig. 1. Interferograms and their difference for two isolated emission lines with slightly different line centers. DASH measures the interferogram within a path difference interval (shown schematically in red) around the optimum path difference (black arrow) for Doppler winds.

The difference between these two fringe patterns is shown in black across the bottom of Fig. 1. This difference is small near zero OPD where the two interferograms have nearly the same phase and is also small at large OPD where the envelope of both fringe patterns is small. Between these two limits (near an OPD of 400 units on Fig. 1) the difference signal is maximum. This is the optimum path difference, L_{OPT}, for the measurement of Doppler winds and is given by

$$L_{OPT} = 2\Delta d_{OPT} = \frac{1}{2\pi\sigma_D} \tag{1}$$

where σ_D is

$$\sigma_D = \sigma_E \sqrt{\frac{kT}{mc^2}} \tag{2}$$

#137013 - $15.00 USD Received 22 Oct 2010; accepted 16 Nov 2010; published 1 Dec 2010
(C) 2010 OSA

In Eq. (2), T is the temperature of the emission line in Kelvin, m is the mass of the emitting species, σ_E is the wavenumber of the emission, *c* is the speed of light, and k is Boltzmann's constant. Typically, the sensitivity of the interferogram to a Doppler shift does not decrease rapidly when measuring away from the optimal OPD, so that other design aspects of the interferometer such as size and mass are likely to be significant when deciding on the OPD interval that is sampled by a specific DASH interferometer.

The stepped Michelson interferometers typically measure only a few phase points covering about one wavelength of total path difference to determine the Doppler winds. Similar to SHS, DASH uses gratings in the arms and an imaging detector to sample the interferogram over a much larger range of path differences. Since the effective wind signal is small at both large and small path differences the range of path differences measured in DASH is close to L_{OPT}. To accomplish this simply requires that one of the gratings in a conventional SHS be placed further from the beam splitter than the other, as shown in Fig. 2.

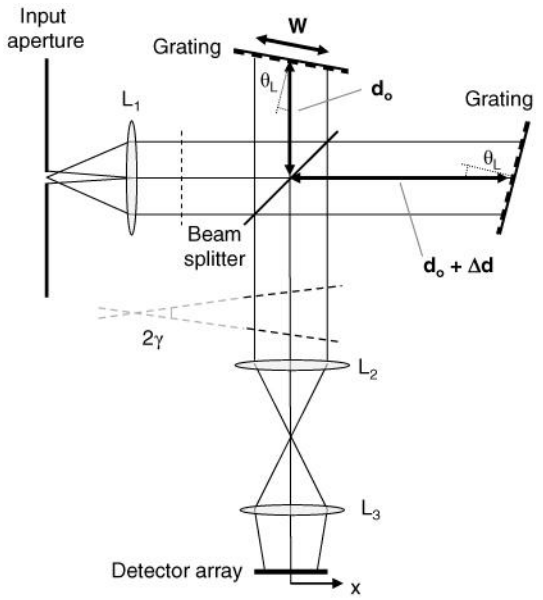

Fig. 2. Schematic of a DASH interferometer from Englert et. al. [10]. Due to the different arm lengths, the path difference interval imaged on the detector array is not centered on zero path difference as in conventional SHS.

To measure the temperature of an emitting species the Michelson technique requires knowledge of the absolute contrast of the fringe pattern at this path difference [4]. As with the Michelson, temperature can be determined with a DASH instrument by measuring the absolute contrast of the fringe pattern at a known path difference. This method, however, requires a detailed characterization of background sources and non-ideal fringe modulation effects. A more robust method of temperature determination is to measure the relative change in fringe contrast across an optical path difference interval. Since DASH measures the interferogram over a large range of path difference, typically a few thousand wavelengths, the envelope of the fringes can change appreciably across the interferogram. This envelope change is less sensitive to background contamination and detailed knowledge of the modulation efficiency of the interferometer.

In addition, the large path difference interval measured by DASH enables it to obtain fringe patterns for multiple emission lines simultaneously. The lines must be separated in wavenumber by enough to result in unique fringe frequencies at the detector for the path difference interval measured. For example, assuming a minimum of 20 fringes between

#137013 - $15.00 USD Received 22 Oct 2010; accepted 16 Nov 2010; published 1 Dec 2010
(C) 2010 OSA

adjacent lines and a detector providing 1000 samples across the interferogram, 25 emission lines could be measured simultaneously. These multiple lines could be from geophysical sources and/or include one or more on-board calibration lines to track instrument drifts simultaneously with each exposure.

4. A DASH for wind and temperature measurements

Figure 3 is a schematic diagram of a DASH interferometer designed for upper atmospheric wind and temperature measurements of the thermospheric F-layer using the 630 nm O[^{1}D] oxygen emission.

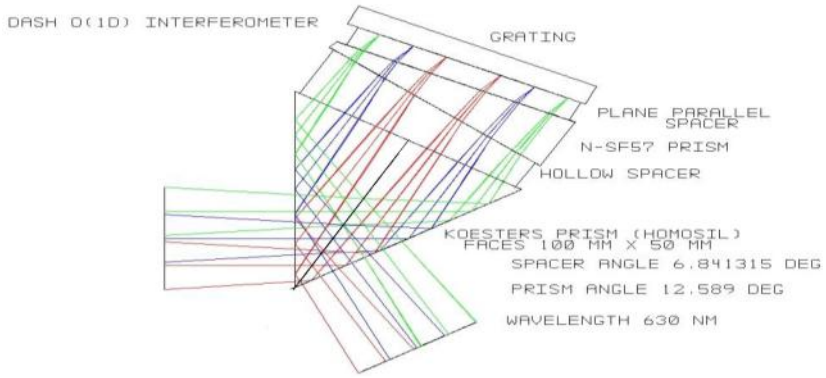

Fig. 3. Schematic of the DASH interferometer for the 630 nm emission. The central blue ray is along the optical axis. The green and red ray bundles are at the edges of the grating aperture.

The interferometer consists of a Köster's double-reflection prism as a beamsplitter, a hollow wedged spacer, field widening prism, parallel spacer and diffraction grating. Although other configurations are possible [6,8,10], the advantage of using the Köster's prism is that the two interferometer beams exit the beamsplitter parallel to each other enabling a design where the two beams sample different apertures of a single spacer, field widening prism and diffraction grating. This quasi-common path configuration is insensitive to translations of the interferometer elements and can easily be assembled as a monolith. The path difference step ($2\Delta d$ in Fig. 2) arises from the different beamsplitter-to-grating distances along the optical axis (central blue ray in Fig. 3) while the path difference interval is determined by the grating angle and aperture. Table 1 shows the design properties of the interferometer.

By using the same grating for both interferometer arms the path difference step and interval are coupled. In order to take advantage of the quasi-common path design while at the same time maximizing the field of view to achieve the highest sensitivity (see section 5, below) and provide at least a 20 fringe difference between the O(^{1}D) line and the nearest atmospheric contaminant (an OH line, see Table 1), the decision was made to sample a path difference between 1.37 cm and 4.79 cm. This is not centered on the optimum path difference of 4.2 cm given by Eq. (1) (for an oxygen temperature of 1000 K), however, as we stated above the amplitude of the fringe difference falls off slowly away from the optimum path difference, so that the penalty for not centering the optical path difference interval on L_{OPT} is small.

#137013 - $15.00 USD Received 22 Oct 2010; accepted 16 Nov 2010; published 1 Dec 2010
(C) 2010 OSA

Table 1. Design properties of the 630 nm DASH interferometer.

O(^{1}D) Interferometer Parameters	
Athermal for vacuum operation	
Beamsplitter	Koester's 100mm (side) x 50mm (thick) Fused Silica (Homosil)
Spacer #1 (Hollow)	Apex angle: 6.84° Fused silica frame strain relieved
Prism	Apex angle: 12.598° Schott N-SF57
Spacer #2 (Plane Parallel)	Fused silica frame strain relieved
Grating	Aperture: 28 x 28 mm active area Field: f/6 (4.5° half-angle cone) Groove density: 900 g/mm Blank: Fused Silica
Path difference sampled	1.37 to 4.79 cm
Optimum path difference	4.2 cm @ 1000K (O(^{1}D), λ = 630 nm)
Number of fringes across field (as built)	
630.4789 nm Ne calibration	42
630.0304 nm O[^{1}D]	81
629.7916 nm OH contaminant	102

4.1.1 Thermal compensation

One of the primary technical challenges associated with interferometers is their thermal stability. In practice, no instrument can be fabricated to be absolutely thermally stable so such drifts must be monitored, quantified, and corrected. This is especially true for Doppler wind measurements where in order to determine winds with a precision of 3 m/s, wavelength changes must be measured to 1 part in 10^8. Although the Köster's prism configuration is insensitive to translation of the interferometer elements, rotation of these same elements will result in changes in fringe frequency and phase and, if not monitored, would result in systematic wind errors. Similarly, thermal changes in the index of refraction of the field widening prism and the groove density of the gratings also produce fringe and phase shifts. By appropriate choice of prism glass and grating substrate these two effects can be made to cancel one another. Compensation is achieved when the index of refraction of the field widening prism *n* and thermal expansion coefficient of the grating blank α_{CTE} are related by:

$$\alpha_{CTE} = -\frac{dn}{dT}\frac{n}{n^2 - 1} \tag{3}$$

where *dn/dT* is the derivative of the prism index with respect to temperature. Equation (3) motivated the choice of N-SF57 for the field widening prism and fused silica for the grating substrate for the DASH interferometer design shown in Fig. 3.

4.2 The monolithic DASH

Generally, DASH interferometers can be fabricated as monolith devices, just as SHS interferometers [9]. A DASH interferometer using a Köster's prism configuration is no exception. Monolithic interferometers are particularly rugged and therefore well suited for

#137013 - $15.00 USD Received 22 Oct 2010; accepted 16 Nov 2010; published 1 Dec 2010
(C) 2010 OSA

field and space applications. A monolithic interferometer requires fixed, hollow spacers in the spaces on either side of the field widening prism. Initially we planned to use fused silica frames for these spacers, however, one of the design issues that surfaced in the fabrication of the monolith was the mechanical strain caused by differential expansion of the N-SF57 prism glass which has a high coefficient of thermal expansion (CTE) and the fused silica beamsplitter and grating substrate which have a much smaller CTE. To allow for differential expansion without undue stress and distortion of the optics, the fused silica hollow spacers surrounding the prism were strain-relieved. The spacers were originally fabricated as frames however, before cementing to the field widening prism a series of cuts were made perpendicular to the face of the frame so that the bonded surface on the prism consisted only of a series of posts or "pickets" on the prism face with gaps between them. After the spacers were bonded to the prism, the cuts were extended all the way through the spacers so the spacers consisted of a series of individual posts. The grating and Köster's prism were then cemented to these posts. In Fig. 4 the posts are evident on either side of the field widening prism.

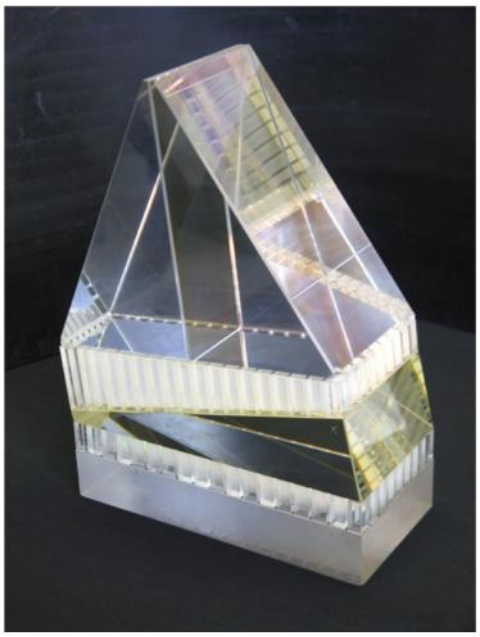

Fig. 4. The monolithic as-built red line DASH interferometer. Hollow spacers on either side of the field widening prism are strain relieved to allow for differential thermal expansion of the interferometer glasses. The triangular edges of the Köster's prism beamsplitter are each 100 mm long.

5. Field of view considerations and laboratory tests

Field widening the interferometer is accomplished by the N-SF57 prism with the apex angle chosen so that from a geometrical optics point of view, the gratings appear to be perpendicular to the optical axis and coincident. Field widening prisms greatly reduce the change in fringe frequency with off axis angle enabling the interferometer to produce high contrast fringes over a much larger cone angle of light. Third order prism aberrations ultimately limit the field of view, however, field widening can commonly achieve étendue gains of two orders of magnitude in both SHS and stepped Michelson interferometers [4,6]. An additional constraint in the choice of prism and spacer angles for the 630 nm DASH interferometer was the desire to simplify the alignment by using a plane parallel spacer between the field widening prism and the grating. The optimum prism angle for N-SF57 glass was determined by ray tracing to be 12.598 degrees with an angle of incidence of 6.840

#137013 - $15.00 USD Received 22 Oct 2010; accepted 16 Nov 2010; published 1 Dec 2010
(C) 2010 OSA

degrees on the beamsplitter side of the prism. This resulted in a maximum field of view in the interferometer of f/6 (4.5 degree half-angle cone) which represents a gain in solid angle of a factor of over 450 compared to a system without field widening operating at the same maximum path difference.

5.1.1 Alignment and fringe frequency tests

The monolithic interferometer was fabricated and aligned at LightMachinery in Ottawa, Ontario. After bonding the spacers to the field widening prism and the prism/spacer assembly to the Köster's prism the final alignment step was to cement the grating to the spacer so that the interferometer produced the desired fringe frequencies for the O(^{1}D) and Ne calibration lines. This was accomplished by monitoring the fringe frequency at the 630.4789 nm Ne line produced by a pen ray lamp during the final cement phase. Subsequent testing at NRL using an optical set-up similar to that described in Englert et. al. [5] determined the fringe frequencies for a number of lines and hence confirmed the design resolution. The as-built fringe frequencies for lines most relevant to the 630 nm airglow measurement are indicated at the bottom of Table 1.

5.1.2 Field of view tests

To verify the solid angle over which the interferometer produces high-contrast fringes the results of a ray trace model were compared with laboratory measurements of the real instrument. The black fringes shown in Fig. 5 illustrate the fringe amplitude vs. path difference predicted by the ray trace model assuming a monochromatic source for both 1.5 degree (f/19) and 4.5 degree (f/6) cone angles of light. The left-hand panel at f/19 illumination shows the model amplitude is nearly constant for all path differences, while the right panel, for an f/6 beam, shows that at the maximum path difference the fringe amplitude is reduced, as expected, by the change in fringe frequency with off-axis angle. We will refer to this effect as the instrument visibility function. Superposed on the modeled fringe patterns in Fig. 5 are measured fringes (red) using an emission line with a finite line width generated by a Ne pen ray lamp. The fringes are recorded with the real instrument using an optical set-up similar to that described in Englert et al. [5] for the same cone angles.

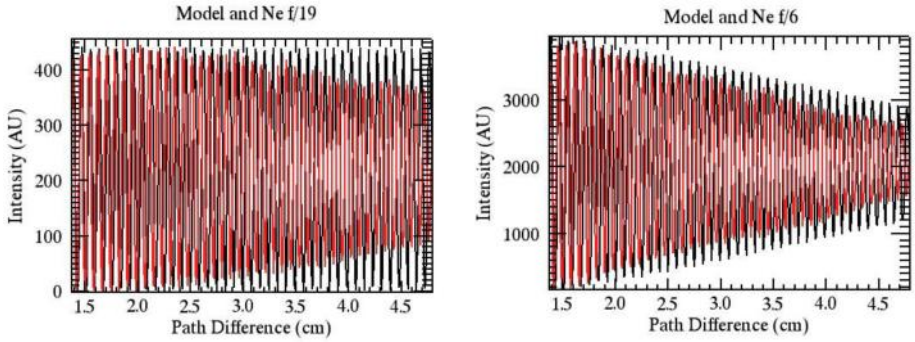

Fig. 5. Modeled (black, monochromatic line) and measured (red, finite line width) fringes for f/19 beam (left) and f/6 beam (right). The decrease in visibility at f/6 is due to the change of fringe frequency with off axis angle. The intensity axis is in arbitrary units. The difference in the modeled and measured fringe patterns can be attributed to the spectral width of the Ne emission line that was used as a source.

The amplitude of the measured fringe patterns (shown in red in Fig. 5) decreases faster with path difference than the model predicts, however, no account has yet been made for the fact that the model assumed a monochromatic source and the Ne pen ray used in the measurements has a finite line width, primarily due to thermal broadening. If, for the f/19 measurements, the real interferometer is assumed to have a constant instrument visibility across all path differences as suggested by the model, the decrease in fringe amplitude shown

#137013 - $15.00 USD Received 22 Oct 2010; accepted 16 Nov 2010; published 1 Dec 2010
(C) 2010 OSA

in red on the left panel is solely due to the line width of the Ne line. Assuming pure thermal broadening, the data from the left panel of Fig. 5 indicates that the temperature broadening of the emission line from the pen ray lamp is equivalent to approximately 900 K. Once the temperature of the line is known, its line width can be incorporated into the model. Figure 6 shows the fringe amplitude vs. path difference at f/6 after the model was corrected for the line width of the source.

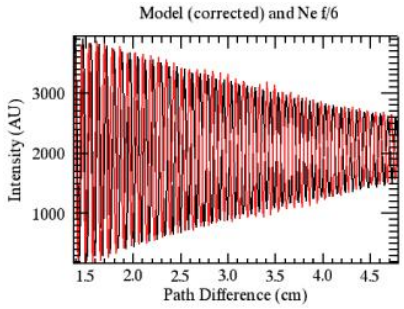

Fig. 6. When the measured source line width is included in the model (black), it is in good agreement with the measurement (red).

6. Thermal soak tests

To determine the dependence of fringe frequency and phase on the interferometer temperature, we performed a series of measurements whereby the interferometer was placed in an aluminum enclosure that was thermally controlled to an accuracy of 0.1 K (see Englert et al. [5] for a more detailed description of the enclosure and optical set up). The temperature of the enclosure was cycled between 28° C and 30° C with a hold time of 12 hours at each temperature over a 95 hour period. Using a Cerium- Argon (Ce-Ar) hollow cathode lamp as a source a fringe pattern was recorded every 30 min resulting in a total of 193 images for the entire data set. The exposure time of each of the images was 20 seconds so that the fringe drift during a single exposure is negligible. The fringes from two Ar lines were monitored to assess the thermal drift of the instrument. The Ar line at 630.7657 nm produced a total of 17 fringes across the interferogram while the line at 629.6873 nm produced 110 fringes. Using the method described in [7] the phase of the fringe patterns vs. path difference was calculated for each of the lines using the average of 50 rows near the center of a fringe image. For perfect, equally spaced fringes the phase vs path difference should be a linear function that increases by 2π radians for every additional fringe across the pattern. In practice, however, fringe distortions lead to curvature in the phase plots (see Englert et al. [5] for examples). These fringe distortions are also commonly seen in SHS interferometers [7] and are due to non-flat surfaces in the interferometer, index inhomogeneities in the interferometer glasses or distortions in the exit optics that images the fringe pattern on the array detector. However, as long as the fringe distortions depend weakly on temperature, the phase distortion determined from one fringe pattern can be used as a reference and subtracted from the others. If this reference phase is subtracted from each line independently the resulting phase plots will represent how the frequency (slope) and phase offset (intercept) of the fringe patterns change with temperature for each line. Figure 7 shows the intercept (left panel) and the slope (right panel) as a function of time for both Ar lines over the entire data set.

#137013 - $15.00 USD Received 22 Oct 2010; accepted 16 Nov 2010; published 1 Dec 2010
(C) 2010 OSA

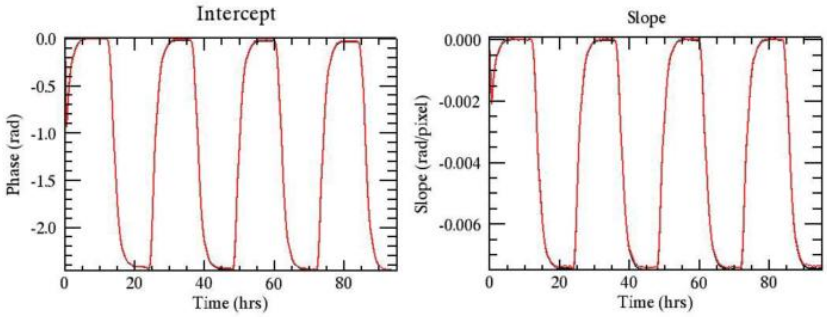

Fig. 7. Changes in the fringe patterns of two Ar lines when the temperature of the interferometer enclosure is cycled between 28° C and 30° C. The left panel shows the intercept shift corresponding to the extrapolated absolute phase at zero path difference, while the right panel shows the slope or frequency change. The traces for the two Ar lines are shown in black and red and are essentially on top of one another.

The temperature transitions are clearly evident in Fig. 7. The left panel shows the phase change in radians extrapolated to zero path difference while the right hand panel shows the change in slope. Both panels use the fringe image nearest 7 hrs as the reference to subtract the linear and nonlinear phase contributions. Data for both Ar lines are shown. The fact that they are superposed on this plot suggests that the thermal drift is not a simple mechanical shift of the external imaging optics or detector position because the two lines have much different spatial frequencies (17 fringes vs 110) and thus a mechanical shift of the detector would result in much different phase changes for the two lines. The stability of the imaging system and detector is expected as the external optics and detector were not thermally cycled during this test.

The magnitude of the phase shift from the left hand panel in Fig. 7 is roughly 2.5 radians per 2°C or 0.40 fringes per 2°C for both Ar lines. The right hand panel indicates a fringe frequency change across the detector of approximately 0.0075 radians/pixel per 2°C. Since there are 512 pixels across the image this corresponds to a change in the total number of fringes of 0.61. These shifts are much larger than we expected from the model calculation that accounts for the thermal expansion of the grating and the thermally induced index change of the field widening prism. The discrepancy is probably due to a rotation of the interferometer elements caused by thermoelastic distortion that results from the vastly different CTE of the glasses. Thermoelastic distortion is not included in the model. It is also clear from Fig. 7 that the fringe frequencies and phases are reproducible with changes in temperature. That is, when the temperature of the interferometer housing cycles, the fringe phase and frequency drift for approximately 4 hours before stabilizing. As discussed above, the DASH interferometer has the ability to measure an internal calibration line with each exposure. When the linear drift of one of the Ar lines is used as a calibration to correct the drift of the other Ar line, the remaining fluctuation in the measured phase at the center of the sampled OPD interval is approximately 1.2 mrad or approximately 1.2 m/s in velocity units for this data set. This is well within the precision required for a meaningful geophysical measurement. Analysis of the data in Fig. 7 also suggests that when the temperature of the interferometer housing is maintained to an precision of 0.1 K with a PID (proportional/integral/derivative) control loop that uses a cycle time of 10 seconds the interferometer temperature fluctuates by only 3 mK due to the poor thermal coupling of the interferometer to the enclosure and its large thermal inertia.

7. Conclusions

We have reported the design and laboratory tests of a thermally compensated monolithic DASH interferometer. Measurements have confirmed that the spectral resolution and étendue of the design have been achieved in the laboratory. We have shown that ± 0.1 K thermal control of the enclosure surrounding the interferometer results in a thermal response at the

#137013 - $15.00 USD Received 22 Oct 2010; accepted 16 Nov 2010; published 1 Dec 2010
(C) 2010 OSA

interferometer of approximately 3 mK. Cycling the interferometer temperature between 28 °C and 30 °C resulted in a larger than expected thermal drift which is likely due to thermo-elastic distortion, however, with appropriate thermal control and the ability to simultaneously monitor calibration sources the precision achieved is commensurate with the measurement of thermospheric winds.

Acknowledgements

This work was supported by the Office of Naval Research. The authors would like to thank Ian Miller and Vaz Zastera of LightMachinery, Ronen Feldman, Andrew N. Straatveit, John F. Moser, W. Layne Marlin, Patrick B. Bell, and Brody Fuchs for their contributions to this work.

#137013 - $15.00 USD Received 22 Oct 2010; accepted 16 Nov 2010; published 1 Dec 2010
(C) 2010 OSA